On Loss-Aware Optimal Control of Wave Energy Converters With Electrical Power Take-Offs

Zechuan Lin ⓘ, *Student Member, IEEE*, Jiayue Zhou ⓘ, *Student Member, IEEE*, Xuanrui Huang ⓘ, *Member, IEEE*,
Kemeng Chen ⓘ, Xi Xiao ⓘ, *Member, IEEE*, and John V. Ringwood ⓘ, *Fellow, IEEE*

Abstract—Incorporating the non-ideal power take-off (PTO) efficiency of wave energy converters (WECs) into energy-maximizing control is crucial for achieving optimal electrical power generation. The majority of previous loss-aware controllers are based on a simplified power-coefficient (PC) model or only consider the copper loss, which remain insufficient to describe a real electrical PTO. In this article, a high-fidelity loss model, encompassing different loss components of the PTO (a generator and a power converter), is developed, and a number of loss-aware model predictive control (MPC) options are derived and compared in a realistic case study. The results highlight the importance of using an appropriate loss model, rather than a PC model, both for power evaluation and for control, and it is shown that a quadratic loss model employed in MPC is effective in approximating the true loss function, so that near-optimal power production can be achieved with fast computation.

Index Terms—Wave energy converter, power take-off, loss model, model predictive control.

I. INTRODUCTION

ADVANCED control of wave energy converters (WECs) can play an important role in improving their power capture efficiency, thereby reducing the levelized cost of wave energy (LCoE). The majority of current WEC controllers use the maximization of mechanical energy, under given system constraints, as the control objective [1], [2]. However, power take-off (PTO) systems that convert mechanical energy into electricity inevitably introduce losses, and the importance of *non-ideal PTO efficiency* has been recognized in a number of studies. Significant power generation drops associated with mechanical-energy-maximizing reactive control, in the presence of PTO losses, are reported in [3], [4], [5], and it is suggested that the 'aggressive' control condition of mechanical energy

maximization, which leads to large reactive power, becomes somewhat futile [6], and improvements in electrical energy require more 'moderate' control behavior, which can be achieved via proper tuning of reactive coefficients [7], or penalty terms on PTO loads [8]. All these results indicate that it is crucial to incorporate PTO losses in control design, namely, to achieve *loss-aware* control.

In the WEC control literature, the typical loss model assumes that loss power is *proportional to* the absolute value of instantaneous mechanical power [9], [10], [11], [12], [13], [14], termed the power-coefficient (PC) model. Accordingly, loss-aware control approaches are proposed, including model predictive control [9], [10], [11], [12], spectral control [13], and moment-based control [14]. However, as will be shown in this study, the PC-assumption is not appropriate for electrical PTOs which, due to their control flexibility and fast response, are particularly suitable for implementing optimal control. For instance, when the WEC (inevitably) reaches large-force and near-zero-velocity regions, the PC model gives a near-zero loss estimate, while the generator actually incurs large copper losses.

A realistic electrical PTO usually includes at least a generator and a power converter, the former subject to copper and iron losses, while the latter has conduction and switching losses. Although copper losses have been *independently* studied in WEC control [15], [16], [17], where they usually appear as a quadratic term in the control objective function, other losses, typically of the same magnitude, should not be ignored. Loss-aware control for WECs needs to be based on a more complete, realistic loss model.

PTO loss modeling can adopt a complete PTO efficiency map [18], [19], obtained from dry testing, or converter losses can be evaluated via power electronics simulation [20]. However, these studies on loss modeling have only been focused on power assessment, without a loss-aware controller design. Importantly, as the actual loss function is generally complex, it is of great importance to investigate its complexity-reduction possibilities so that, after being incorporated in a loss-aware control design, the controller can be *computationally efficient*. Moreover, for PTO designers, it is essential to understand the behavior of PTO losses and loss-aware control, to best ameliorate the loss effects.

In this article, by reviewing existing loss modeling approaches, a high-fidelity PTO loss model encompassing the copper, iron, conduction, and switching losses is developed, which was not detailed in the WEC control literature, and the actual loss characteristics are thereby clarified. Next, a loss

analysis under mechanical energy-maximizing model predictive control (MPC) is conducted for a realistic case study, and the power evaluation results of the developed loss model are compared with the PC model. Then, a nonlinear MPC controller based on the high-fidelity loss model is developed, and an approximate, linear, MPC controller is further proposed, which is more computationally efficient. Finally, the performance of different loss-aware controller options is comprehensively examined. The results provides answers to the following fundamental questions, which have been overlooked in previous studies:

1) *What are the realistic loss characteristics?* It is shown that the loss characteristics of an electrical PTO are fundamentally different from the prevailing PC model, and failure to grasp this distinction will result in inaccuracies in power evaluation and suboptimality in control.

2) *How to handle realistic losses in control?* It is shown that PTO losses can be effectively represented with a quadratic function in the velocity-force domain for loss-aware control, leading to near-optimal performance with faster computation. This *loss approximation* stands as another successful example of *approximate control* for WECs, in addition to approximate modeling [21], approximate solution [22], etc., providing further insights to this direction.

3) *What is the power-improving limit from the control side?* It is revealed that, for a given device, the room for loss-aware control is affected by sea states: Large waves can lead to more 'necessary' losses that cannot be ameliorated by control and, in such a case, more focus should be placed on optimization of the PTO itself. This result provides the basis for possible *control co-design of PTOs*.

The remainder of this article is organized as follows. The WEC system is introduced in Section II. A full PTO loss model is developed in Section III. Loss-aware control options are derived in Section IV. Finally, the cast study results are presented and discussed in Section V.

II. WEC System

The considered WEC system consists of a floating body rigidly linked to a rotary generator through a ball screw, and the generator is connected to a power converter and then to the DC bus. The system schematic is shown in Fig. 1.

A. WEC Body Hydrodynamics

The equation of motion of the oscillating body is described [23] by

$$(m + \mu)a + R_0 v + k_r * v + Kz = f_e + f_g, \tag{1}$$

where z, $v = \dot{z}$, and $a = \ddot{z}$ are the body displacement, velocity, and acceleration, respectively, f_e and f_g are the wave excitation and PTO (generator) forces, m, μ, R_0, and K are the mass, infinite-frequency added mass, friction damping coefficient, and buoyancy force coefficient, while $*$ denotes the convolution operation, and k_r is the radiation retardation function. The convolution term can be described [2] using the following state-space model
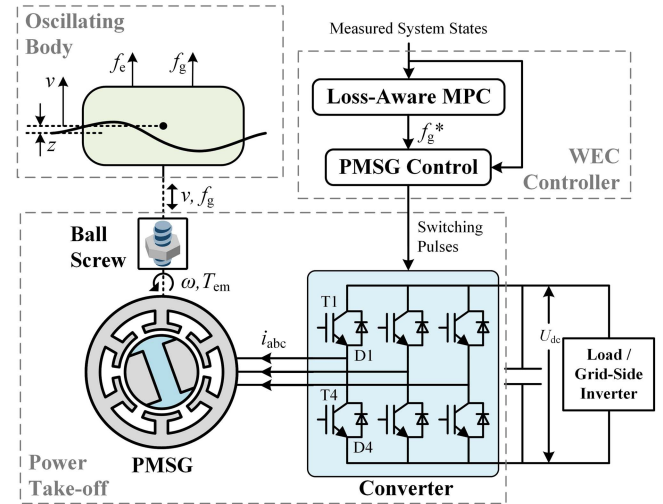
$$\dot{\xi} = A_r \xi + B_r v,$$

Fig. 1.   Schematic of the WEC system.

$$k_r * v = C_r \xi, \tag{2}$$

where $\xi \in \mathbb{R}^L$ is the state of the radiation subsystem, and A_r, B_r, C_r are the associated matrices. Hence, defining the augmented system state as $x = [v, z, \xi^T]^T \in \mathbb{R}^{L+2}$, the overall state-space model is

$$\dot{x} = Ax + Bf_e + Bf_g, \tag{3}$$

where

$$A = \begin{bmatrix} -\frac{R_0}{m+\mu} & -\frac{K}{m+\mu} & -\frac{C_r}{m+\mu} \\ 1 & 0 & 0_{L\times1} \\ B_r & 0_{1\times L} & A_r \end{bmatrix}, \quad B = \begin{bmatrix} \frac{1}{m+\mu} \\ 0 \\ 0_{L\times1} \end{bmatrix}. \tag{4}$$

B. PTO Dynamics

The generator is a rotary permanent-magnet synchronous generator (PMSG) controlled by field-oriented control (FOC). The PMSG voltage equations on the d-q axes are

$$u_d = Ri_d + L_d \frac{di_d}{dt} - N_p \omega L_q i_q$$

$$u_q = Ri_q + L_q \frac{di_q}{dt} + N_p \omega (L_d i_d + \psi), \tag{5}$$

where $u_{d/q}$, $i_{d/q}$ are the voltage and current on the d or q axis, ω is the rotor (mechanical) angular velocity, and N_p, R, L_d, L_q, ψ are the number of pole pairs, resistance, dq-axis inductance, and flux linkage, respectively. The electromagnetic torque T_{em} is

$$T_{em} = \frac{3N_p}{2} \left(\psi i_q + (L_d - L_q) i_d i_q \right). \tag{6}$$

The linear motion of the heaving body and the rotation of the PMSG are linked by the ball screw as follows

$$\omega = \frac{2\pi}{\lambda} v \tag{7}$$

$$T_{em} = \frac{\lambda}{2\pi} f_g, \tag{8}$$

where λ is the lead of the screw.

C. Control Scheme

The WEC control scheme (see Fig. 1) has a two-layer, cascaded structure. The upper layer is the energy-maximizing controller (to be described later), which calculates an optimal PTO force command f_g^*. The lower layer is a PMSG current controller, which produces f_g^* by controlling the q-axis current i_q to track a command i_q^*, while keeping the d-axis current i_d at zero, i.e., $i_{d*} = 0$. The current controller employs a proportional-integral (PI) loop that outputs dq-axis reference voltages, based on the corresponding current errors, and a space-vector pulse width modulation (SVPWM) module that outputs the final switching signals to the converter, based on the reference voltages.

Since the response of the PI current loop is much faster than that of the WEC hydrodynamics, for the upper layer controller, the dynamic current responses can be reasonably neglected. Hence, the PTO can be viewed as an *ideal actuator*. Substituting $i_d = i_d^* = 0$ into (6) and combining (8), the *actual* q-axis current for a given force command f_g^* is

$$i_q = i_q^* = \frac{\lambda}{3\pi N_p \psi} f_g^* \qquad (9)$$

In this study, the dq-variables are defined based on a constant-amplitude Park transformation, so the PMSG current amplitude is $I = |i_q|$. As will be shown in the next section, all PTO losses are functions of two variables, the PMSG speed ω and current I, and they are directly linked to the WEC velocity v and PTO force f_g through (7) and (9).

III. ELECTRICAL PTO LOSSES

In this section, a high-fidelity PTO loss model is developed. Note that, strictly speaking, the 'exact' losses can only be evaluated in real-world testing for the specific WEC device. The focus here, however, is to get as close as possible to the real losses by summarizing main loss sources and the corresponding verified loss models, so as to clarify the loss characteristics, and study the impacts of model and control options.

A. PMSG Losses

PMSG losses generally consist of copper and iron losses (the mechanical loss is included in (1)). The copper loss can simply be described by

$$P_{\text{copper}}(I) = \frac{3}{2} R I^2. \qquad (10)$$

The iron loss is modeled based on Bertotti model [24], where the iron loss density, p_{iron}, at each point of the stator core of PMSG, is calculated as

$$p_{\text{iron}} = k_{\text{hyst}} B_0^\gamma f + k_{\text{eddy}} B_0^2 f^2 + k_{\text{exc}} B_0^{1.5} f^{1.5} \qquad (11)$$

which contains three parts: hysteresis loss, eddy current loss, and excess loss, all related to flux density distribution B_0 and fundamental electrical frequency f, with material coefficient γ, k_{hyst}, k_{eddy} and k_{exc}, respectively. The flux density distribution B_0 is affected by the phase currents and is therefore a function of I. The fundamental electrical frequency f is linked to the rotor speed ω as $f = N_p |\omega|/(2\pi)$. Hence, the total core loss is the

volume integral of the core loss density and can be described by

$$P_{\text{iron}}(\omega, I) = K_{\text{hyst}}(I)|\omega| + K_{\text{eddy}}(I)\omega^2 + K_{\text{exc}}(I)|\omega|^{1.5}, \qquad (12)$$

where K_{hyst}, K_{eddy}, and K_{exc} are current-dependent coefficients of the core loss. In this study, iron loss data are directly computed by finite-element analysis (FEA) on a ω-I grid, from which a fitted iron loss function $P_{\text{iron}}(\omega, I)$ is obtained. In most cases, FEA gives a precise iron loss calculation, provided that the material parameters are accurately given [25].

B. Converter Losses

For an IGBT-based converter shown in Fig. 1, losses generally consist of conduction and switching losses. In this study, analytical converter loss models [26], [27] are employed, which have been experimentally verified to be consistent with the measured losses [27].

Conduction losses are caused by the non-zero voltage drops on both the IGBT and diode when conducting. If the on-state current is I_{on}, the on-state power loss is

$$P_{\text{on,T/D}} = (V_{0,\text{T/D}} + R_{\text{T/D}} I_{\text{on}}) I_{\text{on}}, \qquad (13)$$

where $R_{\text{T/D}}$ and $V_{0,\text{T/D}}$ are the linearized on-state resistance and voltage bias of the IGBT (T) or the diode (D).

Analysis of the conduction loss can be focused on the positive half cycle of the sinusoidal A-phase current, whose average power loss is one-sixth of the total loss. During this half cycle, since the current is positive, it flows either through the upper IGBT, T1, or the lower diode, D4. Let the phase current be $I\cos\theta$, so the voltage drop is $(V_{0,\text{T/D}} + R_{\text{T/D}} I\cos\theta)$. Define $D_a \in [0, 1]$ as the proportion of time that T1 is conducting. The average conduction losses in T1 and D4 are thus

$$P_T = \frac{1}{2\pi} \int_{-\frac{\pi}{2}}^{\frac{\pi}{2}} (V_{0,T} + R_T I \cos\theta) I \cos\theta D_a \mathrm{d}\theta$$

$$P_D = \frac{1}{2\pi} \int_{-\frac{\pi}{2}}^{\frac{\pi}{2}} (V_{0,D} + R_D I \cos\theta) I \cos\theta (1 - D_a) \mathrm{d}\theta, \quad (14)$$

and it remains only to calculate D_a, which is determined by the reference voltage and the modulation method, which is a seven-segment SVPWM in this study. Let the phase voltage be $U\cos(\theta + \phi)$, with U being the voltage amplitude and ϕ being the phase difference between voltage and current, and further define the 'modulation ratio'

$$\alpha = \frac{\sqrt{3} U}{U_{\text{dc}}}. \qquad (15)$$

It can be derived [27] that

$$D_a \approx \frac{1}{2} \left[1 + \alpha \left(\frac{2\sqrt{3}}{3} \cos(\theta + \phi) - \frac{3}{4\pi} \cos(3(\theta + \phi)) \right) \right]. \qquad (16)$$

Substituting (16) into the original integrals in (14), summing up the results, and multiplying by six, the total average conduction loss power can be obtained as

$$P_{\mathrm{cond}}(\omega, I)$$

$$= \left[\frac{3}{\pi}(V_{0,\mathrm{T}}+V_{0,\mathrm{D}})+\alpha\frac{\sqrt{3}}{2}\cos\phi(V_{0,\mathrm{T}}-V_{0,\mathrm{D}})\right]I$$

$$+ \left[\frac{3}{4}(R_{\mathrm{T}}+R_{\mathrm{D}})+\alpha\left(\frac{4\sqrt{3}}{3\pi}\cos\phi-\frac{3}{10\pi^2}\cos(3\phi)\right)\right.$$

$$\left.\times(R_{\mathrm{T}}-R_{\mathrm{D}})\right]I^2. \tag{17}$$

In (17), α and ϕ are determined by the current control requirement. From (5), by assuming a sinusoidal steady state, where $i_{\mathrm{d}}=0$, $\mathrm{d}i_{\mathrm{d}}/\mathrm{d}t=0$ and $\mathrm{d}i_{\mathrm{q}}/\mathrm{d}t=0$, get

$$u_{\mathrm{d}}=-N_{\mathrm{p}}\omega L_{\mathrm{q}}i_{\mathrm{q}}$$

$$u_{\mathrm{q}}=Ri_{\mathrm{q}}+N_{\mathrm{p}}\omega\psi, \tag{18}$$

and

$$\alpha=\frac{\sqrt{3}\sqrt{u_{\mathrm{d}}^2+u_{\mathrm{q}}^2}}{U_{\mathrm{dc}}}$$

$$\phi=\angle(u_{\mathrm{d}}+ju_{\mathrm{q}})/(ji_{\mathrm{q}}), \tag{19}$$

where $j=\sqrt{-1}$, and $\angle$ denotes the angle of a complex number. Equations (17) (18) (19) form the complete conduction loss model. It can be seen that (17) contains first-order and quadratic terms in I, and the associated coefficients both have i) a constant term determined by the parameter *sum* of the IGBT and diode, and ii) a *current-speed-dependent* term originated from the parameter *difference* between the IGBT and diode. The latter term is rather nonlinear, but it will be shown later that its effect is relatively limited.

Switching losses are caused by the transient turn-on and turn-off processes associated with power semiconductor devices. For example, during the IGBT turn-on process, the voltage decreases from an initial value U_{sw} to zero, while the current increases from zero to the target value I_{sw}, with power loss during this interval. The switching loss characteristic of a device can be described by

$$E_{\mathrm{sw,T/D}}=\frac{U_{\mathrm{sw}}}{U_{\mathrm{base}}}(a_{\mathrm{T/D}}I_{\mathrm{sw}}+b_{\mathrm{T/D}}), \tag{20}$$

where $a_{\mathrm{T/D}}$ and $b_{\mathrm{T/D}}$ are the linearized switching loss coefficients and biases, respectively, and U_{base} is the voltage under which the loss parameters are measured. These parameters can be obtained from the appropriate device datasheet.

Similarly, switching loss analysis is also performed on the positive half cycle of the A-phase current, and $I_{\mathrm{sw}}=I\cos\theta$ and $U_{\mathrm{sw}}=U_{\mathrm{dc}}$. During each switching period, the upper IGBT and lower diode both undergo a switching process. So, the average energy loss *per switch* is

$$E_{\mathrm{sw}}=\frac{U_{\mathrm{dc}}}{U_{\mathrm{base}}}\frac{1}{2\pi}\int_{-\frac{\pi}{2}}^{\frac{\pi}{2}}((a_{\mathrm{T}}+a_{\mathrm{D}})I\cos\theta+(b_{\mathrm{T}}+b_{\mathrm{D}}))\mathrm{d}\theta. \tag{21}$$

Then, the average switching loss power is

$$P_{\mathrm{sw}}=E_{\mathrm{sw}}f_{\mathrm{sw}}, \tag{22}$$

where f_{sw} is the switching frequency. Calculating the integral in (21) and multiplying by six, the total average switching loss power is

$$P_{\mathrm{sw}}(I)=\frac{6f_{\mathrm{sw}}U_{\mathrm{dc}}(a_{\mathrm{T}}+a_{\mathrm{D}})}{\pi U_{\mathrm{base}}}I+\frac{3f_{\mathrm{sw}}U_{\mathrm{dc}}(b_{\mathrm{T}}+b_{\mathrm{D}})}{U_{\mathrm{base}}}. \tag{23}$$

It can be seen that the switching loss depends only on the current I, and is an affine function of I.

C. Summary of Losses, and the Power-Coefficient Loss Model

From (10), (12), (17), (23), all the losses are functions of I and ω, and thereby functions of f_{g} and v; summing up them gives the high-fidelity loss function P_{hf}

$$P_{\mathrm{hf}}(f_{\mathrm{g}}, v)=P_{\mathrm{copper}}+P_{\mathrm{iron}}+P_{\mathrm{cond}}+P_{\mathrm{sw}}. \tag{24}$$

Alternatively, the power-coefficient (PC) loss model adopted in, e.g., [14], assumes that the loss is proportional to the absolute value of instantaneous power, depending on the power direction

$$P_{\mathrm{pc}}(f_{\mathrm{g}}, v)=\begin{cases}\beta|f_{\mathrm{g}}v|, & -f_{\mathrm{g}}v\geq 0 \\ \frac{\beta}{1-\beta}|f_{\mathrm{g}}v|, & -f_{\mathrm{g}}v<0\end{cases} \tag{25}$$

where $\beta\in[0, 1)$ is the loss coefficient.

IV. LOSS-AWARE MODEL PREDICTIVE CONTROL

To achieve a loss-aware, energy-maximizing control within PTO constraints, MPC is recognized as an ideal solution [2]. To begin with, using zero-order hold discretization, the continuous-time model of (4) is discretized into

$$x[k+1]=A_{\mathrm{d}}x[k]+B_{\mathrm{d}}f_{\mathrm{e}}[k]+B_{\mathrm{d}}f_{\mathrm{g}}[k], \tag{26}$$

where k is the discrete time index with a sampling time of T_{s}, and $A_{\mathrm{d}}=\exp(AT_{\mathrm{s}})$ and $B_{\mathrm{d}}=A^{-1}(A_{\mathrm{d}}-I)B$ are the system matrices. Using trapezoidal integration, the extracted mechanical energy between the kth and $(k+1)$th instants is

$$E_{\mathrm{mech}}(x[k], f_{\mathrm{e}}[k], f_{\mathrm{g}}[k])=-\frac{1}{2}T_{\mathrm{s}}f_{\mathrm{g}}[k](x_1[k]+x_1[k+1]). \tag{27}$$

Assume that the total PTO loss is described by a loss function P_{loss}, then the electrical energy loss during this process is

$$E_{\mathrm{loss}}(x[k], f_{\mathrm{e}}[k], f_{\mathrm{g}}[k])$$

$$=T_{\mathrm{s}}P_{\mathrm{loss}}\left(f_{\mathrm{g}}[k], \frac{1}{2}(x_1[k]+x_1[k+1])\right), \tag{28}$$

where the average velocity between the kth and $(k+1)$th step is used for the calculation. On the other hand, the operational constraints include i) the maximum body displacement Z_{m}, ii) the maximum body velocity V_{m}, and iii) the maximum PTO force F_{m}. Then, a MPC controller can be derived which, at each step, solves for an optimal control force sequence over a prediction horizon, such that it maximizes the extracted *electrical* energy while keeping the system within the constraints. This can be expressed as the following optimization problem

$$\max_{\bar{f}_{\mathrm{g}}[0],\ldots,\bar{f}_{\mathrm{g}}[N-1]}\sum_{i=0}^{N-1}E_{\mathrm{mech}}(\bar{x}[i], \bar{f}_{\mathrm{e}}[i], \bar{f}_{\mathrm{g}}[i])$$

$$- \sum_{i=0}^{N-1} E_{\mathrm{loss}}(\bar{x}[i], \bar{f}_{\mathrm{e}}[i], \bar{f}_{\mathrm{g}}[i]),$$

$$\text{s.t. } \bar{x}[i+1] = A_{\mathrm{d}}\bar{x}[i] + B_{\mathrm{d}}\bar{f}_{\mathrm{e}}[i] + B_{\mathrm{d}}\bar{f}_{\mathrm{g}}[i], \quad i = 0, \ldots, N-1$$

$$-Z_{\mathrm{m}} \le \bar{x}_2[i] \le Z_{\mathrm{m}}, \quad i = 1, \ldots, N$$

$$-V_{\mathrm{m}} \le \bar{x}_1[i] \le V_{\mathrm{m}}, \quad i = 1, \ldots, N$$

$$-F_{\mathrm{m}} \le \bar{f}_{\mathrm{g}}[i] \le F_{\mathrm{m}}, \quad i = 0, \ldots, N-1$$

$$\bar{x}[0] = x[k], \quad \bar{f}_{\mathrm{e}}[i] = f_{\mathrm{e}}[k+i], \quad i = 0, \ldots, N-1, \quad (29)$$

where $\bar{f}_{\mathrm{g}}[0], \ldots, \bar{f}_{\mathrm{g}}[N-1]$ is the (virtual) control sequence to be solved, and $\bar{x}[0], \ldots, \bar{x}[N]$ is the corresponding system trajectory. At the kth instant, the trajectory starts from the currently measured state $x[k]$ and is subject to the predicted wave excitation force sequence $f_{\mathrm{e}}[k], \ldots, f_{\mathrm{e}}[k+N-1]$. After the optimal control sequence is determined, the first move will be applied to the device, namely $f_{\mathrm{g}}[k] = \bar{f}_{\mathrm{g}}[0]$ while, at the next step, a new optimization problem, for a shifted horizon, is built and solved again.

Clearly, the choice of loss function plays a central role in the specific loss-aware control solution. In this study, MPC (29) with four individual loss function choices is examined:

1) *MPC using no loss function (MPC):* In this case, the loss term is simply zero, i.e., $P_{\mathrm{loss}}(f_{\mathrm{g}}, v) = 0$, and the controller maximizes mechanical energy. This is the conventional WEC MPC formation. The optimization to be solved online is a quadratic program.

2) *MPC with the high-fidelity loss model (hf-LAMPC):* This corresponds to a perfect model matching, i.e., $P_{\mathrm{loss}}(f_{\mathrm{g}}, v) = P_{\mathrm{hf}}(f_{\mathrm{g}}, v)$. However, the nonlinear loss function results in a nonlinear program, posing a major challenge for online computation.

3) *MPC with a quadratic loss model (quad-LAMPC):* To reduce the computational burden, it is desirable to keep the problem as a quadratic program. Hence, it is proposed to approximate the loss function with a quadratic function

$$P_{\mathrm{loss}}(f_{\mathrm{g}}, v) = \alpha_{\mathrm{f}} f_{\mathrm{g}}^2 + \alpha_{\mathrm{v}} v^2, \quad (30)$$

where α_{f} and α_{v} are the associated coefficients.

4) *MPC with the PC loss model (pc-LAMPC):* Alternatively, the PC loss model can be used in the objective function, i.e., $P_{\mathrm{loss}}(f_{\mathrm{g}}, v) = P_{\mathrm{pc}}(f_{\mathrm{g}}, v)$, as in [14]. However, pc-LAMPC also leads to nonlinear programming.

V. CASE STUDY

A. Setup

A realistic WEC scenario is considered:

1) *Wave condition:* The target sea area is Wheat Island, East China Sea [28]. The occurrences and wave energy distribution of different sea states, represented by the significant wave height (Hs) and peak period (Tp), are shown in Fig. 2(a) and (b). In the following tests, representative sea states will be selected, and the corresponding waves will be simulated using a Bretschneider spectrum with random-phase realizations in the time domain.
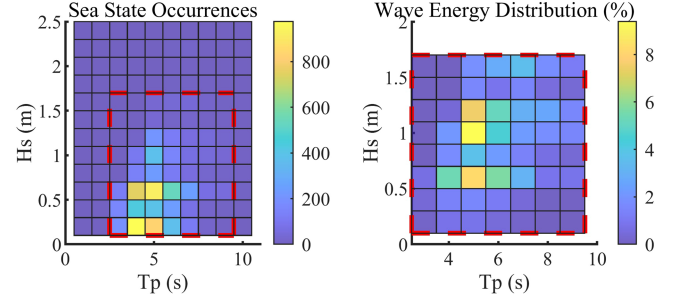

Fig. 2. Sea state occurrence and wave energy distribution of Wheat Island, East China Sea, in 2021 [28].

TABLE I
PMSG PARAMETER VALUES

Parameter	Value	Unit
R	3.55	mΩ
$L_{\mathrm{d}}, L_{\mathrm{q}}$	531, 878	μH
ψ	0.2313	Wb
N_{p}	4	—

TABLE II
POWER CONVERTER PARAMETER VALUES

Parameter	Value	Unit
$R_{\mathrm{T}}, R_{\mathrm{D}}$	1.46, 1.58	mΩ
$V_{0,\mathrm{T}}, V_{0,\mathrm{D}}$	0.75, 0.75	V
$a_{\mathrm{T}}, a_{\mathrm{D}}$	0.163, 0.06	mJ/A
$b_{\mathrm{T}}, b_{\mathrm{D}}$	7.0, 10.0	mJ
$V_{\mathrm{base}}, V_{\mathrm{dc}}$	600, 600	V
f_{sw}	10	kHz

2) *WEC body:* The considered body is a vertical cylinder with a radius of 2 m and a draught of 2 m. This size is chosen according to the dominant wavelength of the sea area. Its hydrodynamic parameters are calculated using NEMOH [29].

3) *PTO:* The maximum displacement is $Z_{\mathrm{m}} = 2$ m, equal to the body draught. The ball screw has a lead of 40 mm. Simulations under a MPC controller are first conducted to determine the typical operating range and, according to this range, realistic PMSG parameters are obtained by conducting a brief generator design process based on finite-element analysis (FEA). The design objective is to make the PMSG range match the optimal control requirement. This yields a 187.5 kW PMSG, whose basic parameters are listed in Table I; specifically, the iron loss map is also acquired from the FEA model. The maximum velocity and PTO force are 2.34 m/s and 177 kN, set to be 1.5 times the rated values. The power converter is based on the 1200 V Infineon FF600R12KE7 IGBT module, selected according to the PMSG operating range. The conduction and switching parameters are obtained from the relevant datasheet [30] and summarized in Table II. Finally, the overall PTO efficiency map is shown in Fig. 3, which yields a 95% efficiency at the rated operating point.
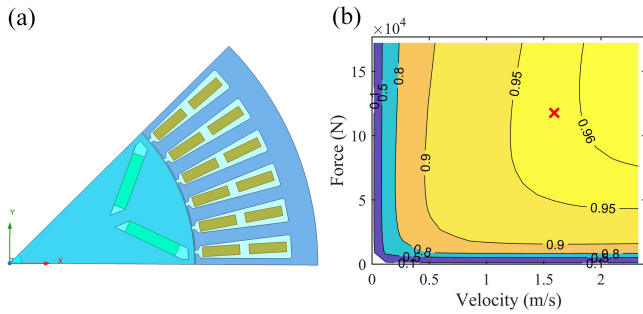
Fig. 3.   The PTO system. (a) FEA model of the PMSG. (b) The total efficiency map, including the PMSG and converter. The red cross represents the rated operating point. Note that all losses of the PTO are represented as functions of body velocity (generator speed (7)) and PTO force (PMSG current (9)).
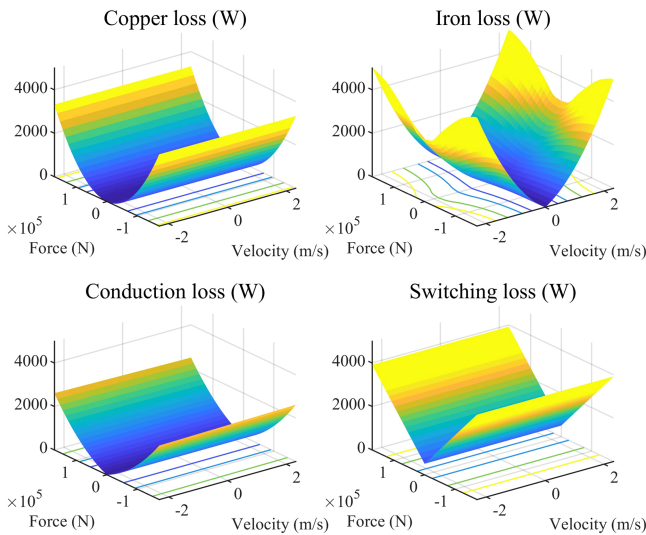

Fig. 4.   Loss maps of the four loss components. Note the contrast between the velocity force dependency of the iron loss compared to other loss components, which are predominantly force dependent.

Note that, in the following case study, the hydrodynamic system (1) is simulated, and the 'actual' losses are evaluated by the high-fidelity loss function.

For the MPC controllers, the sampling time for prediction is T_s=0.2 s, while the prediction horizon N is chosen to be 36, giving a 7.2-second prediction (time) horizon. As a typical feature of MPC for WECs, the power capture performance increases with N and finally reaches an asymptotic limit, so N should be sufficiently large. It is verified that N=36 meets this requirement under all the considered conditions in the following study.

B. Loss Evaluation

The loss contours of the copper, iron, conduction, and switching loss components are plotted in Fig. 4. As already indicated in (10) and (23), the copper and switching losses depend on the PTO force (current) only. The conduction loss depends primarily on the force as well, which means that the velocity (speed)-dependent terms in (17) are negligible. On the other hand, the iron loss (12) is mainly determined by velocity and also affected,
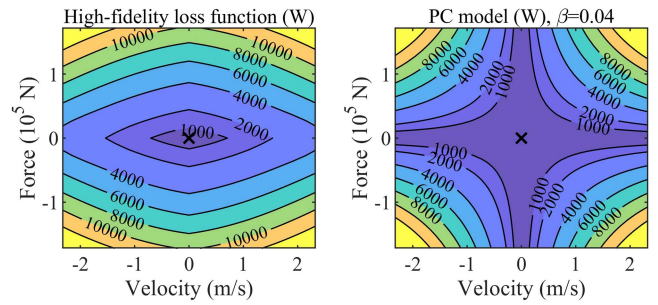

Fig. 5.   The high-fidelity loss function (left) displays a significantly different shape than the PC model (right).
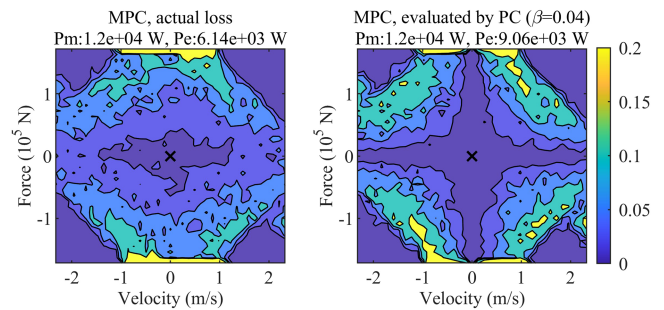

Fig. 6.   Loss distribution (%) of the MPC trajectory, evaluated by the high-fidelity loss function (left) and a PC model (right). Pm: Average mechanical power. Pe: Average electrical power.

to a lesser extent, by force. Summing up the losses, the contour of the total PTO loss is shown in Fig. 5(a), which exhibits a near-elliptical shape and, within the operating range displayed in Fig. 5, the PTO force has a much greater impact on losses. In contrast, the contour of the PC loss model, with $\beta = 0.04$, is shown in Fig. 5(b), which exhibits a hyperbolic shape. Specifically, in high-force, low-velocity and low-force, high-velocity regions (namely, low-power regions), the PC model gives a near-zero loss estimate, overlooking the fact that simply maintaining a high PTO force with no generator motion, or making the generator rotate at a high speed without applying any current, both result in a high electrical losses. This fundamental difference indicates that a PC model cannot grasp the true loss characteristics of an electrical PTO.

To illustrate the impact of loss models, a MPC trajectory is simulated under Hs = 1 m and Tp = 6 s, and the loss distributions evaluated by the high-fidelity loss model, and a PC model, are shown in Fig. 6. One can see that the two models give different loss distributions; particularly, true losses are more concentrated on the large-force, low-velocity region, which indicates that the large actions used by MPC are the main source of losses. In contrast, the losses evaluated by the PC model deviate to high-power regions and this deviation, as will be shown next, will inevitably lead to errors in the final power evaluation.

A comprehensive comparison of power evaluation is conducted for the different loss models, and the results are shown in Fig. 7. The test includes different sea states and three controllers: MPC, optimal damping, and an optimal reactive controller, whose control parameters are set according to [22]. For MPC, it
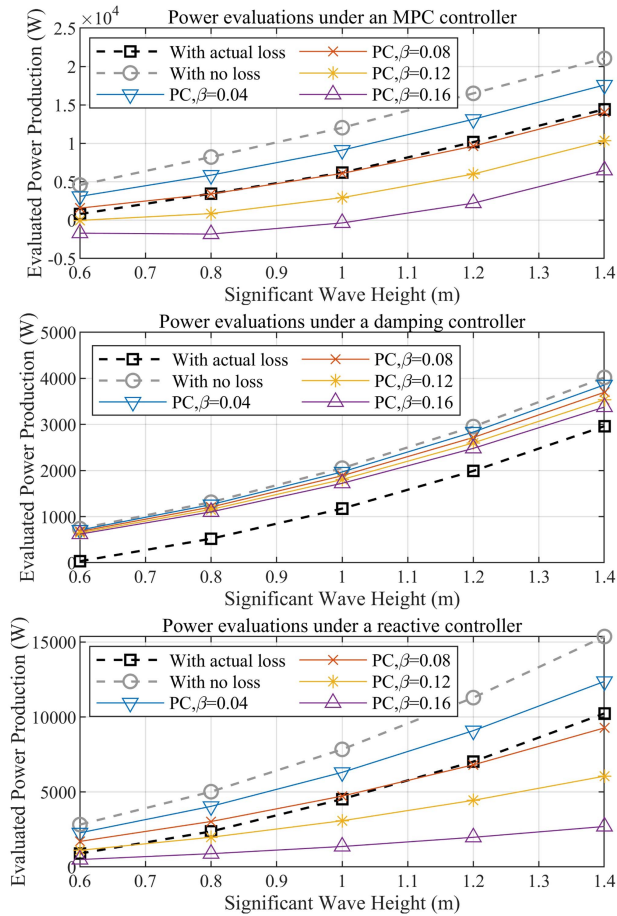
Fig. 7. Power evaluations using different loss models, under different sea states (Tp = 6 s) and three controllers.
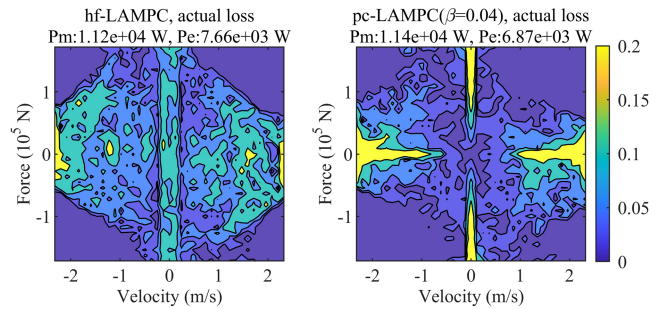

Fig. 8. Actual loss distribution (%) of hf-LAMPCs (left) is more dispersed, while that of pc-LAMPC (right) is concentrated in low-power regions. Pm: Average mechanical power. Pe: Average electrical power.

C. Loss-Aware Optimal Control

Now, two loss-aware controllers, the hf-LAMPC and pc-LAMPC, are tested with Hs = 1 m and Tp = 6 s, and the (actual) loss distributions are shown in Fig. 8(a) and (b), respectively. Compared to the MPC loss distribution in Fig. 6(a), it can be seen that hf-LAMPC restricts the trajectory so that losses are not concentrated in high-force regions but shift toward low-force regions and become dispersed. Consequently, the average electrical power increases from 6.14 kW to 7.66 kW. Also note that the mechanical power decreases from 12 kW to 11.2 kW, which is only an intermediate link in the wave-to-wire chain and has minor relevance to the final, usable energy. In contrast, the pc-LAMPC alters the distribution of losses in a different manner—concentrating them in low-power regions. This is because the controller perceives low losses in these areas but, as shown in Fig. 5, the reality is quite the opposite. Consequently, electrical power generation, 6.87 kW, remains sub-optimal.

The effectiveness of hf-LAMPC and pc-LAMPC is now comprehensively tested under different sea states, and the results are shown in Fig. 9. Note that the hf-LAMPC always represents the performance limit, whereas pc-LAMPC always remains sub-optimal, no matter how the loss coefficient β is tuned. In particular, recall that $\beta = 0.08$ yields a quite good power evaluation under MPC in Fig. 7, but when employed in loss-aware control, performance degradation becomes inevitable. Moreover, sometimes pc-LAMPC performs even more poorly than MPC with no loss model (e.g., when Tp = 7 s and Hs = 1.2–1.4 m); in such cases, the incorrect loss model used in control has a *negative* impact.

Another important observation is that, as the wave amplitude increases, MPC performance naturally increases, while the performance improvement from MPC to hf-LAMPC lessens; in other words, less room is left for the control side to save power loss with large waves. This can be explained by the fact that, with small waves, the displacement constraint is inactive, and the peak-to-average ratio of power is high under MPC. In this situation, WEC oscillation amplitude can be restricted to sacrifice a little mechanical power capture, but greatly save PTO losses. On the contrary, with large waves, the system oscillation is already restricted by constraints and, in order to capture power, some losses are necessary. In general, this control limit is determined by the PTO; further improvements in efficiency can
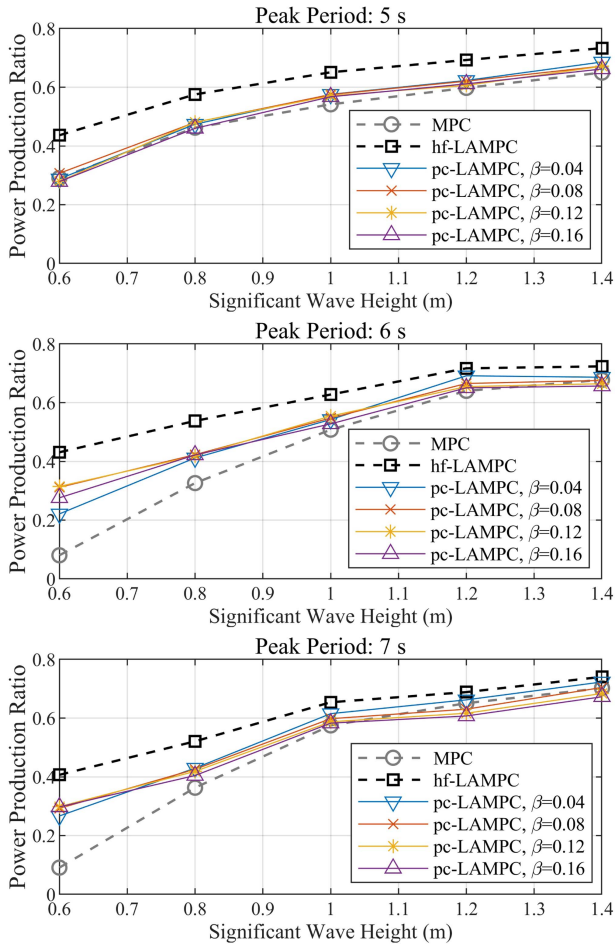
can be seen that a PC model with $\beta = 0.08$ gives power estimates close to the true values. However, the same power coefficient yields obvious errors under reactive control, especially for small waves (e.g., Hs = 0.6 m). Moreover, under damping control, the PC model cannot represent the actual loss, always overestimating power, no matter how β is tuned. Hence, it can be concluded that a PC model cannot be accurate for all sea states and for all controllers, due to mismatches in loss characteristics representation.

Revisiting Fig. 7 (top), one can also see that MPC, with optimal mechanical power generation, yields low net electrical power, especially for small waves (e.g., when Hs = 0.6 m, the electrical power is near zero). Even for large waves, e.g., Hs = 1.4 m, the electrical efficiency remains less than 70%, much lower than the 95% rated efficiency shown in Fig. 3. This observation means that the rated PTO efficiency can be very misleading in a WEC application; a WEC typically experiences continuous oscillations, inevitably passing through low-efficiency regions, and significant losses will occur if no measure is taken to reduce them. For PTO designers, an efficiency improvement could involve an enlargement of high-efficiency regions, or a manipulation of operating point through, e.g., a gear system, as discussed in [18]. Another (simultaneous) measure is through loss-aware control, which will be studied next.

Fig. 9. Performance limits of controllers. Here, the 'power production ratio' is defined as the ratio of average electrical power to *the maximum mechanical power*.
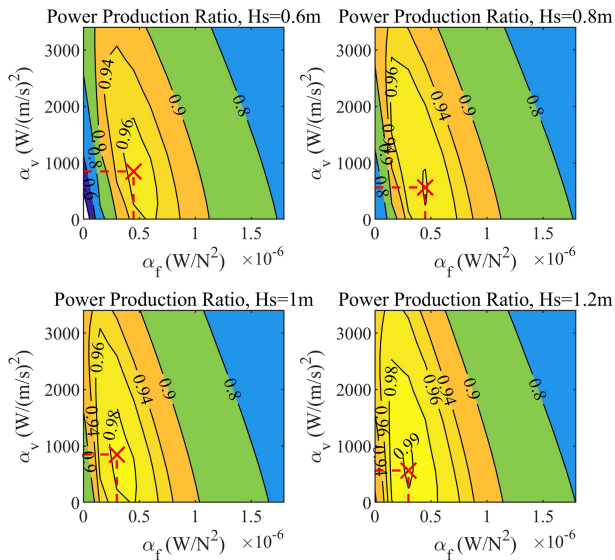

Fig. 10. Performance of different quadratic coefficients in quad-LAMPC (Tp = 6 s). Here, the 'power production ratio' is defined as the ratio of electrical power generation to that of *the hf-LAMPC*.
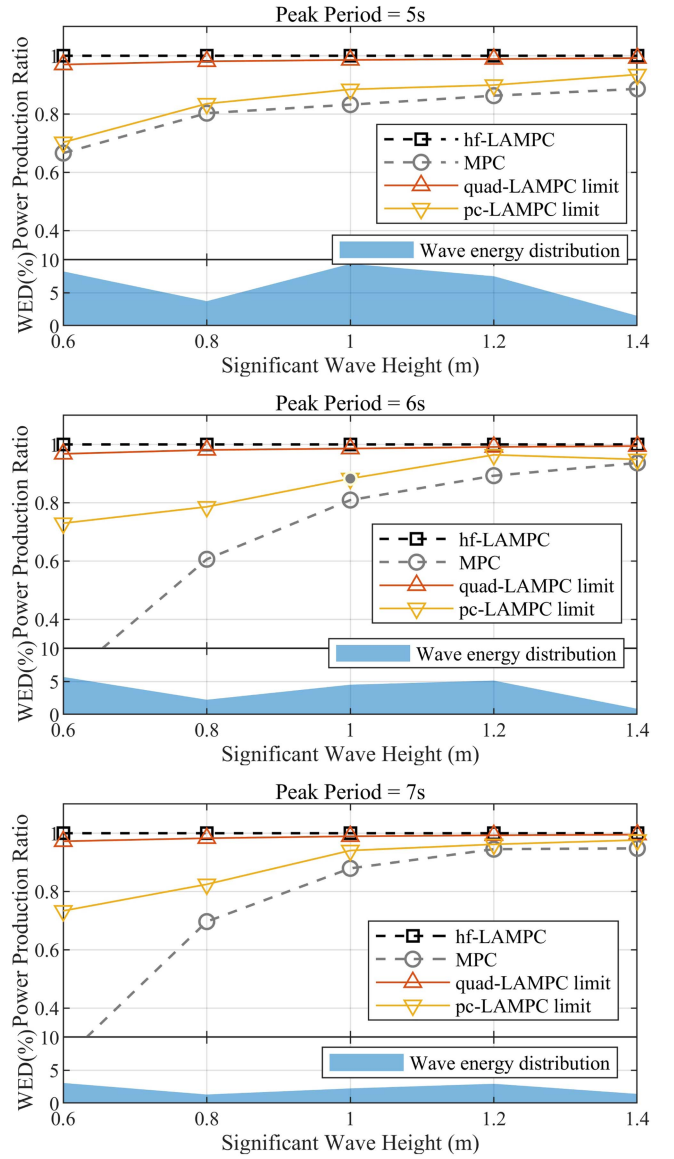

Fig. 11. Performance limits of loss-aware controllers. Here, the 'power production ratio' is defined as the ratio of electrical power generation to that of *the hf-LAMPC*. Also shown are the wave energy distributions (WED) of different sea states.

only be achieved through optimization of the *physical* PTO itself. Hence, the hf-LAMPC can play an important role in PTO design: PTO performance should be evaluated using hf-LAMPC, in order to identify the efficiency limit of the current device, and PTO optimization should be based on the operating range of hf-LAMPC, rather than other controllers, since they display significantly different loss distributions, as shown in Figs. 6 and 8. This enters the field of *control co-design* [1].

D. Approximate Loss-Aware Control

The hf-LAMPC sets the performance limit, but its implementation requires solving nonlinear programming in real time, which may exceed the computation capability of some controller hardware/software, creating the need for quad-LAMPC, as an approximate, faster, control option. To apply quad-LAMPC,
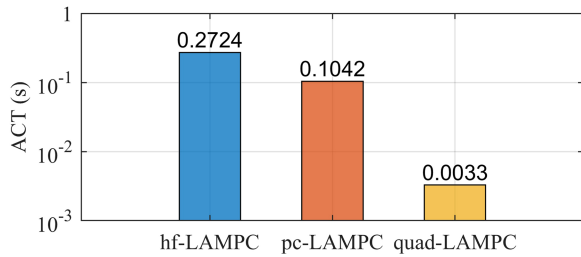
Fig. 12. Average computation time (ACT) of loss-aware controllers.

the quadratic coefficients α_f, α_v should be properly selected. The performance of different coefficients, under four sea states, are shown in Fig. 10. It can be seen that there exists a unique peak performance and, accordingly, a set of best coefficients; however, the best coefficients vary with the sea state, because the sea state, as a description of ocean wave conditions, determines the system operating range. This suggests that, in practical application, the quadratic coefficients should be tuned according to the current sea state. In practice, the mapping from sea states to the optimal coefficients can be computed, offline, into a look-up table, so that the coefficients can be scheduled online in response to changing sea states. Sea state information can be obtained, e.g., from the device motion through an estimator [31]. As the sea state is a relatively long-term parameter, the control cost function only needs to be updated at an infrequent rate, maximally every 20 minutes. However, the requirement for sea state information is a limitation of quad-LAMPC.

Comprehensive testing is then conducted for the four controllers: MPC, hf-LAMPC, pc-LAMPC with the best power coefficient, and quad-LAMPC with the best quadratic coefficients, with the results shown in Fig. 11, where hf-LAMPC is regarded as the performance limit. It is verified that quad-LAMPC is an effective approximation of hf-LAMPC, with over 98% electrical power generation for most of the sea states, outperforming pc-LAMPC, whose loss model is fundamentally different from the high-fidelity loss function, and MPC, where no loss is considered.

Finally, the average computation times are shown in Fig. 12. In the simulation, the implementation of hf-LAMPC and pc-LAMPC are based on the 'fmincon' function of MATLAB, while quad-LAMPC adopts 'quadprog' function. The simulation is conducted on an Intel i7-13700H @2.4 GHz processor. It can be seen that quad-LAMPC requires 100 times less computing time than hf-LAMPC, whereas pc-LAMPC does not show a significant computation advantage over hf-LAMPC, since it still leads to nonlinear programming. Hence, when the computation capability cannot support hf-LAMPC, quad-LAMPC is an ideal control option.

VI. CONCLUSION

In this article, electrical PTO losses and loss-aware optimal control are studied based on a realistic WEC scenario. First, it is crucial to use an accurate loss model for *power evaluation*. The PC model differs fundamentally in parametric structure from the high-fidelity loss function. The latter is near-elliptical

in the velocity-force domain, while the former is hyperbolic. Consequently, they give different loss distributions and power evaluations. A PC model, regardless of how its power coefficient is tuned, cannot maintain accuracy under different sea states and different controllers. Second, it is crucial to use the correct loss model for *loss-aware control*. Hf-LAMPC achieves an improvement in net electricity generation, compared to MPC with no loss, while pc-LAMPC always remains sub-optimal and can even lead to negative impacts. Third, loss-aware control, based on a quadratic loss function, namely quad-LAMPC, proves effective, provided that the optimal set of quadratic coefficients is properly selected according to the current sea state. Quad-LAMPC can achieve over 98% performance for most sea states while reducing the computation time by about a factor of 100; however, the requirement for sea state information remains a main limitation. Finally, the loss-saving limit from the control side is affected by sea states: For small waves, less energy is lost by control, but the efficiency limit is also low; for large waves, the limit is higher, but the room for control also diminishes. Further loss reduction, beyond this limit, can only be achieved by optimizing the PTO itself. Hence, loss-aware control can play an important role in *control co-design* of PTOs, which is a valuable direction for future research.

REFERENCES

[1] J. V. Ringwood, S. Zhan, and N. Faedo, "Empowering wave energy with control technology: Possibilities and pitfalls," *Annu. Rev. Control*, vol. 55, pp. 18–44, 2023.

[2] N. Faedo, S. Olaya, and J. V. Ringwood, "Optimal control, MPC and MPC-like algorithms for wave energy systems: An overview," *IFAC J. Syst. Control*, vol. 1, pp. 37–56, 2017.

[3] E. Tedeschi, M. Carraro, M. Molinas, and P. Mattavelli, "Effect of control strategies and power take-off efficiency on the power capture from sea waves," *IEEE Trans. Energy Convers.*, vol. 26, no. 4, pp. 1088–1098, Dec. 2011.

[4] R. Genest, F. Bonnefoy, A. H. Clément, and A. Babarit, "Effect of non-ideal power take-off on the energy absorption of a reactively controlled one degree of freedom wave energy converter," *Appl. Ocean Res.*, vol. 48, pp. 236–243, 2014.

[5] M. C. Sousounis and J. Shek, "Wave-to-wire power maximization control for all-electric wave energy converters with non-ideal power take-off," *Energies*, vol. 12, no. 15, 2019, Art. no. 2948.

[6] G. Bacelli, R. Genest, and J. V. Ringwood, "Nonlinear control of flap-type wave energy converter with a non-ideal power take-off system," *Annu. Rev. Control*, vol. 40, pp. 116–126, 2015.

[7] A. F. Falcão and J. C. Henriques, "Effect of non-ideal power take-off efficiency on performance of single-and two-body reactively controlled wave energy converters," *J. Ocean Eng. Mar. Energy*, vol. 1, pp. 273–286, 2015.

[8] N. M. Tom, F. Madhi, and R. W. Yeung, "Power-to-load balancing for heaving asymmetric wave-energy converters with nonideal power take-off," *Renewable Energy*, vol. 131, pp. 1208–1225, 2019.

[9] A. Karthikeyan, M. Previsic, J. Scruggs, and A. Chertok, "Non-linear model predictive control of wave energy converters with realistic power take-off configurations and loss model," in *Proc. IEEE Conf. Control Technol. Appl.*, 2019, pp. 270–277.

[10] P. Tona, H.-N. Nguyen, G. Sabiron, and Y. Creff, "An efficiency-aware model predictive control strategy for a heaving buoy wave energy converter," in *Proc. 11th Eur. Wave Tidal Energy Conf.*, Nantes, France, 2015.

[11] P. Andersen, T. S. Pedersen, K. M. Nielsen, and E. Vidal, "Model predictive control of a wave energy converter," in *Proc. IEEE Conf. Control Appl.*, 2015, pp. 1540–1545.

[12] T. Kovaltchouk, F. Rongère, M. Primot, J. Aubry, H. B. Ahmed, and B. Multon, "Model predictive control of a direct wave energy converter constrained by the electrical chain using an energetic approach," in *Proc. 11th Eur. Wave Tidal Energy Conf.*, 2015.

[13] A. Mérigaud and P. Tona, "Spectral control of wave energy converters with non-ideal power take-off systems," *J. Mar. Sci. Eng.*, vol. 8, no. 11, 2020, Art. no. 851.

[14] N. Faedo, G. Giorgi, J. V. Ringwood, and G. Mattiazzo, "Nonlinear moment-based optimal control of wave energy converters with non-ideal power take-off systems," in *Proc. Int. Conf. Offshore Mechanics Arctic Eng.*, vol. 85932, 2022, Art. no. V008T09A082.

[15] A. de la Villa Jaén et al., "Considering linear generator copper losses on model predictive control for a point absorber wave energy converter," *Energy Convers. Manage.*, vol. 78, pp. 173–183, 2014.

[16] A. S. Haider, T. K. Brekken, and A. McCall, "Real-time nonlinear model predictive controller for multiple degrees of freedom wave energy converters with non-ideal power take-off," *J. Mar. Sci. Eng.*, vol. 9, no. 8, 2021, Art. no. 890.

[17] Y. Lao, J. T. Scruggs, A. Karthikeyan, and M. Previsic, "Discrete-time causal control of a wave energy converter with finite stroke in stochastic waves," *IEEE Trans. Control Syst. Technol.*, vol. 30, no. 3, pp. 1198–1214, May 2022.

[18] X. Zhou, S. Zou, W. W. Weaver, and O. Abdelkhalik, "Assessment of electrical power generation of wave energy converters with wave-to-wire modeling," *IEEE Trans. Sustain. Energy*, vol. 13, no. 3, pp. 1654–1665, Jul. 2022.

[19] M. F. Pettersen, "Effect of a non-ideal power take-off system on the electrical power output of a wave energy converter under passive control," M.S. thesis, Dept. Electric Power Eng., Norwegian Univ. Sci. Technol., Trondheim, Norway, 2020.

[20] M. Penalba, J.-A. Cortajarena, and J. V. Ringwood, "Validating a wave-to-wire model for a wave energy converter–Part II: The electrical system," *Energies*, vol. 10, no. 7, 2017, Art. no. 1002.

[21] M. Richter, M. E. Magana, O. Sawodny, and T. K. Brekken, "Nonlinear model predictive control of a point absorber wave energy converter," *IEEE Trans. Sustain. Energy*, vol. 4, no. 1, pp. 118–126, Jan. 2013.

[22] Z. Lin, X. Huang, and X. Xiao, "Fast model predictive control system for wave energy converters with wave tank tests," *IEEE Trans. Ind. Electron.*, vol. 70, no. 7, pp. 6887–6897, Jul. 2023.

[23] W. Cummins et al., "The impulse response function and ship motions" Dept. Navy, David Taylor Model Basin Bethesda, MD, USA, Tech. Rep. 1661, 1962.

[24] G. Bertotti, "General properties of power losses in soft ferromagnetic materials," *IEEE Trans. Magn.*, vol. 24, no. 1, pp. 621–630, Jan. 1988.

[25] J. Du, X. Wang, and H. Lv, "Optimization of magnet shape based on efficiency map of IPMSM for EVs," *IEEE Trans. Appl. Supercond.*, vol. 26, no. 7, Oct. 2016, Art. no. 0609807.

[26] S. M. Sharkh, M. A. Abu-Sara, G. I. Orfanoudakis, and B. Hussain, *Power Electronic Converters for Microgrids*. Hoboken, NJ, USA: Wiley, 2014.

[27] Y. Zhu, M. Xiao, X. Su, G. Yang, K. Lu, and Z. Wu, "Modeling of conduction and switching losses for IGBT and FWD based on SVPWM in automobile electric drives," *Appl. Sci.*, vol. 10, no. 13, 2020, Art. no. 4539.

[28] "National marine data center, national science and technology resource sharing service platform of China," Accessed: Apr. 10, 2023. [Online]. Available: http://mds.nmdis.org.cn/

[29] R. Kurnia and G. Ducrozet, "NEMOH: Open-source boundary element solver for computation of first-and second-order hydrodynamic loads in the frequency domain," *Comput. Phys. Commun.*, vol. 292, 2023, Art. no. 108885.

[30] "Infineon," Accessed: Dec. 16, 2023. [Online]. Available: https://www.infineon.com/cms/en/product/power/igbt/igbt-modules/ff600r12ke7/

[31] S. A. Sirigu, G. Bracco, M. Bonfanti, P. Dafnakis, and G. Mattiazzo, "On-board sea state estimation method validation based on measured floater motion," *IFAC-PapersOnLine*, vol. 51, no. 29, pp. 68–73, 2018.

Zechuan Lin (Student Member, IEEE) was born in Fujian Province, China, in 1996. He received the B.E. degree in electrical engineering from North China Electrical Power University, Beijing, China, in 2019. He is currently working toward the Ph.D. degree in electrical engineering with Tsinghua University, Beijing, China. From 2023 to 2024, he was with the Centre for Ocean Energy Research, Maynooth University, Maynooth, Ireland, where he was a Visiting Student. His research interests include control and control co-design of wave energy converters.

Jiayue Zhou (Student Member, IEEE) was born in Guangdong, China, in 1997. She received the B.Sc. degree in electrical engineering and chinese literature from Tsinghua University, Beijing, China, where she is currently working toward the Ph.D. degree. Her research interests include multi-physics design, optimization and control of ultra-high-speed permanent magnet machines, and design of high-speed resolvers.

Xuanrui Huang (Member, IEEE) was born in Xinjiang Province, China, in 1991. He received the B.E. and Ph.D. degrees in electrical engineering from Tsinghua University, Beijing, China, in 2013 and 2020, respectively. He is currently a Postdoctor with the Department of Electrical Engineering, Tsinghua University. His research interests include permanent-magnet synchronous motor control, wave energy, and switched reluctance machines.

Kemeng Chen was born in Chongqing City, China, in 1999. She received the B.E. degree in 2022 from Tsinghua University, Beijing, China, where she is currently working toward the Ph.D. degree. Her research interests include wave energy and grid integration of renewable energy.

Xi Xiao (Member, IEEE) was born in Hunan Province, China, in 1973. He received the B.E., M.E., and Ph.D. degrees in electrical engineering from Saint Petersburg State Technical University, Saint Petersburg, Russia, in 1995, 1997, and 2000, respectively. Since 2001, he has been with the Department of Electrical Engineering, Tsinghua University, Beijing, China, where he is currently a Full Professor. His research interests mainly include permanent magnet synchronous motor control, power electronics, and renewable energy.

John V. Ringwood (Fellow, IEEE) received the Diploma in electrical engineering from the Technological University, Dublin, Ireland, in 1981, and the Ph.D. degree in control systems from Strathclyde University, Glasgow, U.K., in 1985. From 1985 to 2000, he was with the School of Electronic Engineering, Dublin City University, Dublin, Ireland, also held Visiting positions with Massey University, Auckland, New Zealand, and The University of Auckland, Auckland, New Zealand. From 2001 to 2006, he was the Founding Head with the Department of Electronic Engineering, Maynooth University, and was the Dean of Engineering. He is currently Chair Professor of electronic engineering and the Director with the Centre for Ocean Energy Research, Maynooth University, Maynooth, Ireland. He is also a co-author of the monograph *Hydrodynamic Control of Wave Energy Devices* (with Umesh Korde). His research interests include control systems and its applications, focusing on renewable energy systems (and wave energy in particular), physiology, and exercise physiology. Dr. Ringwood was co-recipient of the IEEE 2016 Control Systems Outstanding Paper Award and 2023 IEEE Transaction on Control Systems Technology Outstanding Paper Award. He is an Associate Editor for IEEE TRANSACTION ON SUSTAINABLE ENERGY, *Journal of Ocean Engineering and Marine Energy*, and *IET Renewable Power Generation*. He is also a Chartered Engineer and the Fellow of Engineers Ireland.